

Characterization of Effective Half-Life for Instant Single-Time-Point Dosimetry Using Machine Learning

Carlos Vinícius Gomes¹⁻³, Yizhou Chen¹, Isabel Rauscher⁴, Song Xue^{1,5}, Andrei Gafita^{4,6}, Jiayi Hu¹, Robert Seifert¹, Lorenzo Mercogli¹, Julia Brosch-Lenz^{4,7}, Jimin Hong¹, Marc Ryhiner¹, Sibylle Ziegler^{8,9}, Ali Afshar-Oromieh¹, Axel Rominger¹, Matthias Eiber⁴, Thiago Viana Miranda Lima^{2,10}, and Kuangyu Shi¹

¹Department of Nuclear Medicine, Inselspital, Bern University Hospital, University of Bern, Bern, Switzerland; ²Institute of Radiology and Nuclear Medicine, Lucerne University Teaching and Research Hospital, Lucerne, Switzerland; ³Graduate School for Cellular and Biomedical Sciences, University of Bern, Bern, Switzerland; ⁴Department of Nuclear Medicine, School of Medicine, Technical University Munich, Klinikum Rechts der Isar, Munich, Germany; ⁵Division of Nuclear Medicine, Department of Biomedical Imaging and Image-Guided Therapy, Vienna General Hospital, Medical University of Vienna, Vienna, Austria; ⁶Ahmanson Translational Theranostics Division, Department of Molecular and Medical Pharmacology, UCLA, Los Angeles, California; ⁷Institute of Nuclear Medicine, Glen Burnie, Maryland; ⁸Department of Nuclear Medicine, Hannover Medical School (MHH), Hannover, Germany; ⁹Department of Nuclear Medicine, LMU University Hospital, LMU Munich, Munich, Germany; and ¹⁰Faculty of Health Sciences and Medicine, University of Lucerne, Lucerne, Switzerland

Single-time-point (STP) image-based dosimetry offers a more convenient approach for clinical practice in radiopharmaceutical therapy (RPT) compared with conventional multiple-time-point image-based dosimetry. Despite numerous advancements, current STP methods are limited by the need for strict and late timing in data acquisition, posing challenges in routine clinical settings. This study introduces a new concept of instant STP (iSTP) dosimetry, achieved by predicting the effective half-life (T_{eff}) of organs using machine learning applied on pretherapy patient data (PET and clinical values). **Methods:** Data from 22 patients who underwent pretherapy ⁶⁸Ga-gallium *N,N*-bis[2-hydroxy-5-(carboxyethyl)benzyl]ethylenediamine-*N,N*-diacetic acid (⁶⁸Ga)Ga-PSMA-11) imaging and subsequently [¹⁷⁷Lu]Lu-PSMA I&T RPT were analyzed. A machine learning model was developed for T_{eff} predictions for the left and right kidneys, liver, and spleen subsequently used to estimate time-integrated activity and absorbed dose. iSTP results were compared against multiple-time-point and previously proposed Hänscheid methods. Our method comprised 2 different prediction scenarios, using data before each therapy cycle and from the first cycle. **Results:** The iSTP method introduced early posttherapy time points (2, 20, 43, and 69 h) for the left kidney, right kidney, liver, and spleen. Dosimetry in the first scenario, aggregating 2 and 20 h, achieved mean differences in time-integrated activity below 27% for all organs. To assess the feasibility, these time points were compared with the best results from the Hänscheid method (kidneys, 69 h; liver and spleen, 20 h). At 2 h, a significant difference ($P < 0.001$) was found for almost all organs except for the spleen ($P = 0.1370$). However, at 20 h, no significant differences were found for the right kidney, liver, and spleen, apart from the left kidney ($P < 0.01$). In the scenario using only the initial PET/CT data to predict T_{eff} for subsequent cycles, iSTP dosimetry achieved no statistical significance ($P > 0.05$) for all cycles in comparison to results using PET data before each therapy cycle. **Conclusion:** Our preliminary results prove the concept for prediction of T_{eff} with pretherapy data and achieving STP shortly and flexibly after the RPT. The

proposed method may expedite the application of dosimetry in broader contexts, such as outpatient or short-duration inpatient treatment.

Key Words: radiopharmaceutical therapy; [¹⁷⁷Lu]Lu-PSMA I&T; machine learning; single time point; dosimetry

J Nucl Med 2025; 00:1-7

DOI: 10.2967/jnumed.124.268175

Dosimetry in radiopharmaceutical therapies (RPTs) is essential to ensure that treatments are effective and safe, which is based on extensive research and clinical trials (1-4). The accepted approach to account for the radiopharmaceutical biodistribution relies on the acquisition of multiple SPECT images at different time points after injection of the radiopharmaceutical, known as the multiple-time-point (MTP) method. Challenges of this method include limited resources, high costs, scarce scanner availability, and patient burdens, potentially increasing overall treatment costs (5-9). Despite these hurdles, evidence underscores dosimetry's role in tailoring treatment strategies more precisely (10,11).

The adoption of single-time-point (STP) image-based dosimetry instead of the MTP method has become accepted and pursued alternatively because of its practicality based on 1 single posttherapy scan. The STP methods proposed by Madsen et al. (5) and Hänscheid et al. (12), which initially focused on neuroendocrine tumors, were expanded to prostate-specific membrane antigen (PSMA)-targeting radiopharmaceuticals (8,9). However, this method presents time-dependency limitation that would influence its clinical use (5-8,12-15). Hou et al. cautioned about the method's accuracy and emphasized its dependence on both radiopharmaceutical and patient specifics (14). Additionally, Brosch-Lenz et al. (8) and Hou et al. (14) suggested that STP dosimetry might not suit all organs or tissues in specific therapeutic contexts. Furthermore, the decision of whether therapy-personalized dosimetry should focus on sparing organs at risk or maximizing lesion absorbed dose remains a point of consideration. This is particularly relevant in the context of significant variations in tumor effective half-lives (T_{eff}), for which the limitations of STP approaches might be more pronounced, as previously documented (14).

Received Jun. 3, 2024; revision accepted Feb. 20, 2025.

For correspondence or reprints, contact Kuangyu Shi (kuangyu.shi@unibe.ch).

Published online Mar. 20, 2025.

Immediate Open Access: Creative Commons Attribution 4.0 International License (CC BY) allows users to share and adapt with attribution, excluding materials credited to previous publications. License: <https://creativecommons.org/licenses/by/4.0/>. Details: <https://jnm.snmjournals.org/page/permissions>.

COPYRIGHT © 2025 by the Society of Nuclear Medicine and Molecular Imaging.

Current limitations in STP dosimetry, particularly in commercial applications, stemmed largely from their dependence on the time point of the SPECT scan for dose evaluation. Kratochwil et al. (16) suggested that scintigraphy performed 1–2 d after infusion served as an effective imaging follow-up for PSMA-positive lesions, reinforcing the relevance of a single scan for dosimetry. Additionally, differences in patient discharge might influence the availability of late-imaging time points. Patients stay in the hospital for a 48-h period in Switzerland during which imaging could be performed. On the other hand, patients receive posttherapeutic scans 24 h after each treatment cycle in Singapore (17).

To address these challenges, the present article introduces an instant STP (iSTP) method based on pretherapy patient data, building on the assumption that the T_{eff} is a patient-intrinsic characteristic (8,14,18), allowing flexible dosimetry with a single measurement during an early scan time point spanning from day 0 to day 3 after injection of the therapy. Our development aims to achieve flexible and iSTP dosimetry after RPT.

MATERIALS AND METHODS

Patient Cohort and Dosimetry Methods

Patient Samples. Twenty-two patients with metastatic castration-resistant prostate cancer underwent [^{177}Lu]Lu-PSMA I&T (^{177}Lu -PSMA I&T; mean injected activity, 7.3 ± 0.3 GBq) RPT at Klinikum Rechts der Isar, Technische Universität München, Germany. In total, 44 therapy cycles were included, comprising pretherapy ^{68}Ga -gallium *N,N*-bis[2-hydroxy-5-(carboxyethyl)benzyl]ethylenediamine-*N,N*-diacetic acid (^{68}Ga -PSMA-11; mean injected activity, 119.0 ± 25.1 MBq) PET/CT scans before each therapy cycle (1, 2, 3, 4, 5, and 9) and SPECT/CT scans at MTPs after injection, further referred to as t_{sc} in hours (at 2, 20, 43, 69, 144, and >165 h, with a minimum of 3 and a maximum of 5 time points). This dataset has been previously reported (19,20). The general characteristics of the patients are detailed in Table 1. In accordance with the local ethics committees in Germany, the institutional review board of the Technische Universität München (reference no. 115/18) approved this study, and all subjects provided written informed consent. All patient data were pseudoanonymized.

Supplemental Table 1 details the number of patients grouped by cycle and time points (supplemental materials are available at <http://jnm.snmjournals.org>).

Data Acquisition and Preparation. Volumes of interest including the left kidney, right kidney, liver, spleen, and urinary bladder were segmented from pretherapy CT images, from which the SUV_{mean} of the organs was extracted. From posttherapy CT images, the left kidney, right kidney, liver, and spleen were used for dosimetric analysis. Segmentation and quantification were performed using SurePlan MRT (MIM Software), requiring manual corrections when necessary (www.mimsoftware.com).

Time-Integrated Activity (TIA): MTP. The pharmacokinetics of ^{177}Lu -PSMA I&T were modeled separately in the left and right kidneys, liver, and spleen, using the following biexponential function:

$$A(t) = A_1 e^{-(\lambda_1 + \lambda_{\text{phys}})t} - A_2 e^{-(\lambda_2 + \lambda_{\text{phys}})t}, \quad \text{Eq. 1}$$

where A_1 is the organ activity (MBq), A_2 is the initial activity, λ_1 and λ_2 are the biological decay constants, and λ_{phys} is the physical decay of ^{177}Lu (6.65 d). Parameters A_2 and λ_2 were considered as population mean data, as described in Supplemental Table 2. Equation 1 was fitted to cycles with at least 3 posttherapeutic SPECT time points to estimate the T_{eff} and TIA (also referred as \tilde{A}) (Eq. 2):

$$\tilde{A} = \int_0^{\infty} A_1 e^{-(\ln(2)/T_{\text{eff}})t} - A_2 e^{-(\lambda_2 + \lambda_{\text{phys}})t} dt. \quad \text{Eq. 2}$$

TIA: STP

Two approaches have been selected to estimate TIA: characterization by the predicted T_{eff} and an initial activity (A_0) (Eq. 3) and utilization of the method by Hänscheid et al. (Eq. 4) (12). Note that time point t_{sc} refers to the specific time point of the SPECT image acquisition in hours. A detailed demonstration of \tilde{A}_{iSTP} can be found in the supplemental materials.

$$\tilde{A}_{\text{iSTP}} = \int_0^{\infty} A_0 \times e^{-(\ln(2)/T_{\text{eff}})t} dt, \quad \text{Eq. 3}$$

$$\tilde{A}_{\text{H}} = \frac{1}{\ln 2} \times A(t_{\text{sc}}) \times 2 \times t_{\text{sc}}. \quad \text{Eq. 4}$$

The STP methods were henceforth referred to as iSTP and Hänscheid, as illustrated in Figure 1. However, the Hänscheid method was developed to incorporate scan time points within a range of 0.75 to 2.5 times the T_{eff} of an organ (including 20, 43, and 69 h t_{sc}). It is

TABLE 1
General Characteristics of Patients per Therapy Cycle, Represented as Mean Values of Age, Weight, PSA Level, LDH, Creatinine, and Hemoglobin

Parameter	Characteristics per cycle			
	Cycle 1	Cycle 2	Cycle 3	Cycle ≥ 4
Number of patients	20	12	6	4
Age (y)	69 ± 9	69 ± 9	69 ± 9	69 ± 9
Weight (kg)	82.3 ± 10.6	82.3 ± 10.6	82.3 ± 10.6	82.3 ± 10.6
PSA (ng/mL)*	714.59	591.35	611.67	438.19
LDH [†]	328.05	275.25	270.83	247.67
Creatinine [‡]	1.0	0.9	0.9	0.9
Hemoglobin [§]	11.52	10.78	10.45	10.72

*PSA levels minimum and maximum values, 0.1 and 2936 ng/mL.

[†]LDH minimum and maximum values, 161.0 and 664.0.

[‡]Creatinine minimum and maximum values, 0.5 and 2.0.

[§]Hemoglobin minimum and maximum values, 8.7 and 15.2.

PSA = prostate-specific antigen; LDH = lactate dehydrogenase.

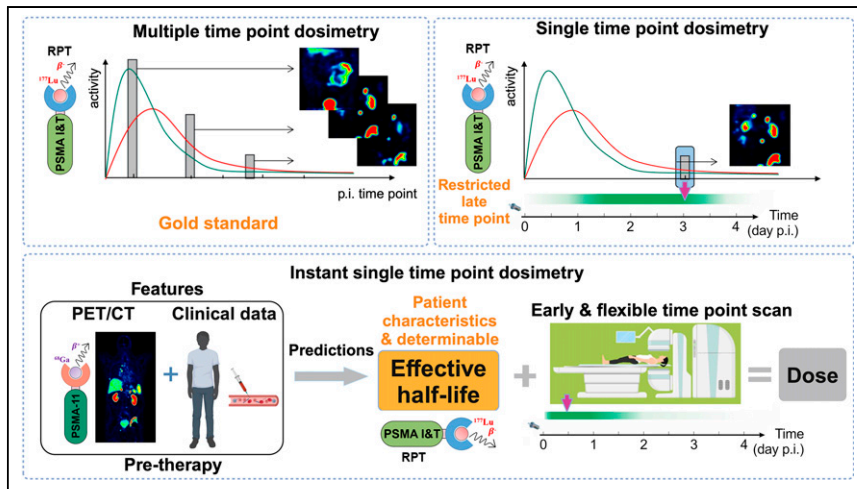


FIGURE 1. Concept of iSTP dosimetry in radiopharmaceutical therapy, encompassing MTP and STP methods. p.i. = postinjection.

important to note that the calculated organ values at 2 h t_{sc} for this method were used in this study for reference only.

Absorbed Dose. Dosimetry was performed for the left kidney, right kidney, liver, and spleen using the iSTP and Hanscheid methods (www.opendose.org). The absorbed dose ($D(r_T, T_D)$), in Grays, in a given target region (r_T) over a dose-integration period (T_D), referred by the product between the $\tilde{A}(r_S, T_D)$, in the source tissue (r_S), and the absorbed dose per decay ($S(r_T \leftarrow r_S)$) (21); is determined:

$$D(r_T, T_D) = \sum_{r_S} \tilde{A}(r_S, T_D) S(r_T \leftarrow r_S). \quad \text{Eq. 5}$$

Machine Learning–Based Model: Development and Validation

The machine learning–based model was developed by incorporating PET imaging quantification, clinical features, and the correspondent T_{eff} of the target organ (left and right kidneys, liver, and spleen). For each specific organ (left and right kidneys, liver, and spleen), a data matrix was defined on the basis of the patient cycle. In this matrix, an individual patient cycle is represented by rows, and their corresponding features form the columns. The selected features (F_i) for the organs (supplemental materials) were derived from not only basic patient characteristics but also pretherapy PET/CT metrics, such as organ SUV_{mean} . In addition, the matrix integrated relevant clinical data (Table 1), all of which are curated and structured according to organ T_{eff_i} function:

$$T_{eff_i} = \text{SVR}(F_i \{ \text{patient characteristic, PET data, clinical data} \}). \quad \text{Eq. 6}$$

We used support vector regression (SVR) (Scikit-learn) as a predictive method for regression, using a radial basis function kernel to construct a hyperplane in high-dimensional space while minimizing error and controlling model complexity. To enhance generalization, standard scaling was applied to the features, ensuring zero mean and unit variance. The hyperparameters C and ϵ were optimized to balance prediction accuracy and model robustness, preventing overfitting and effectively capturing underlying data trends. The SVR was chosen because it provided a superior fit for the small datasets involved in this study (22,23).

The model validation was conducted using k -fold cross-validation. The dataset was partitioned into a k of 10 folds. The error function for model performance evaluation was computed as the mean percentage error between the predicted and measured T_{eff} . Ultimately, the performance was summarized by calculating the mean and SD of the mean error (ME) across the folds.

Clinical Robustness

The robustness of the developed iSTP model was evaluated in 2 scenarios: a model dependency on the time points of the post-therapy SPECT scan, which is a known limitation of the currently used STP method, and a model dependency on the pretherapy ^{68}Ga -PSMA-11 PET/CT before the therapy cycle.

The first scenario computed the organ TIA dependence on the time point of the ^{177}Lu -PSMA I&T SPECT/CT. Our method included pretherapeutic data before each cycle as a feature, as indicated in Equation 6.

The second scenario of our study evaluated the case in which PET/CT pretherapy imaging would be performed only once for the entire treatment. For this purpose, we used pretherapy data from the first cycle to train our machine learning model for predicting subsequent cycles.

Analysis

To estimate the relative absolute differences (RADs), we used the following equation:

$$\text{RAD} = \left| \frac{\theta_{\text{STP}}}{\theta_{\text{MTP}}} - 1 \right| \times 100\%, \quad \text{Eq. 7}$$

where θ_{MTP} and θ_{STP} are estimated values in TIA and absorbed dose from the standard MTP and STP (iSTP and Hanscheid) methods, respectively. Statistical significance was determined at a P value of less than 0.05; otherwise, the results were considered nonsignificant.

RESULTS

Dosimetry and T_{eff}

The MTP-based absorbed doses and T_{eff} results that served as the reference gold standard are shown in Table 2, used for the evaluation of different STP methods.

iSTP: Machine Learning–Based Model Development and Validation

Based on our model’s predictions, the SVR model estimated the organ’s T_{eff} with an ME of $24.4\% \pm 7.4\%$ for the left kidney, $27.2\% \pm 10.0\%$ for the right kidney, $22.7\% \pm 9.8\%$ for the liver, and $19.7\% \pm 5.4\%$ for the spleen. Figure 2 shows the relation of T_{eff} results, depicting the MTP and the predicted values. Statistical analysis using the Wilcoxon signed-rank test indicated no statistical significance for all organs ($P = 0.55, 0.28, 0.87,$ and 0.89 for the left kidney, right kidney, liver, and spleen, respectively).

TABLE 2
Absorbed Dose and T_{eff} Results for Left Kidney, Right Kidney, Liver, and Spleen, Presented as Mean \pm SD, with Minimum and Maximum Values

Organ	Absorbed dose (Gy)	T_{eff} (h)
Left kidney	3.7 ± 1.9 (0.8–8.3)	35 ± 16 (7–65)
Right kidney	3.7 ± 1.9 (0.9–8.6)	34 ± 16 (7–65)
Liver	0.07 ± 0.04 (0.02–0.23)	11 ± 4 (6–25)
Spleen	0.7 ± 0.4 (0.2–1.6)	9 ± 4 (5–25)

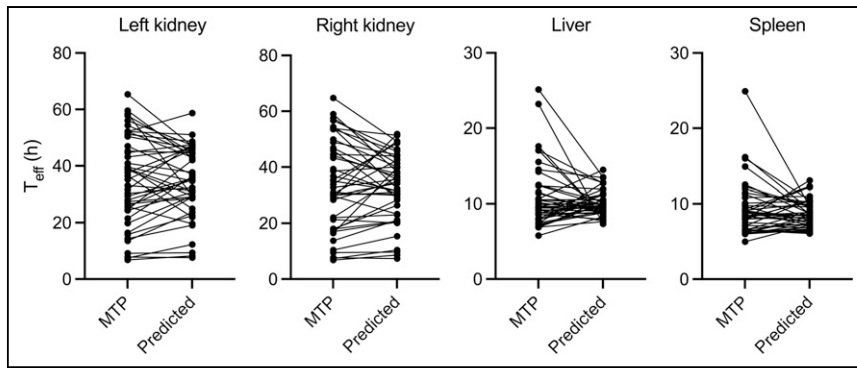


FIGURE 2. Relation between MTP and predicted T_{eff} for left kidney, right kidney, liver, and spleen across all therapy cycles.

STP: Time-Point Independence

Dosimetry was conducted (Eq. 5), wherein the respective TIAs were computed using 2 distinct methods: the iSTP model by applying the predicted T_{eff} (Eq. 3) and the Hanscheid method (Eq. 4). The results in the TIA, presented as RADs per organ, were benchmarked against MTPs (Eq. 7).

The iSTP method, at 2, 20, 43, and 69 h t_{sc} , resulted in mean RADs in TIA of $19.5\% \pm 15.4\%$ and $22.3\% \pm 17.4\%$ for the left and right kidneys, respectively. Differences of $21.2\% \pm 18.9\%$ and $23.4\% \pm 22.5\%$ were observed for the liver and spleen, respectively. However, the Hanscheid method presented RADs of $18.2\% \pm 13.5\%$ for the left kidney and $17.4\% \pm 13.9\%$ for the right kidney, followed by $17.8\% \pm 16.4\%$ and $27.4 \pm 20.3\%$ for the liver and spleen, respectively, considering 20, 43, and 69 h t_{sc} . The nonpaired Mann–Whitney test was performed for all organs, showing statistically nonsignificant differences ($P > 0.05$).

Robustness: Time-Point Dependency

RADs in TIA were calculated from the iSTP and Hanscheid methods against the MTP organized per early time point after injection (aggregating 2, 20, 43, and 69 h) for the left kidney, right kidney, liver, and spleen. Figure 3 shows the RAD values for both methods along with the statistical analysis.

Data for all organs were analyzed using the iSTP method. For the left kidney, at 2 h, this method showed a mean RAD of $25.0\% \pm 15.9\%$, which decreased to $17.4\% \pm 13.5\%$ at 20 h. The lowest errors were observed at 43 h ($11.0\% \pm 15.5\%$) and 69 h ($15.0\% \pm 13.5\%$) t_{sc} .

The iSTP performed similarly for both kidneys. For the right kidney, at 2 h t_{sc} , a mean difference of $27.3\% \pm 17.0\%$ was observed. At 20, 43, and 69 h, the RAD errors were $18.6\% \pm 15.6\%$, $17.3\% \pm 19.5\%$, and $20.6\% \pm 19.8\%$, respectively.

Regarding the liver, this method presented a RAD of $22.1\% \pm 19.3\%$ at 2 h t_{sc} . At 20 h t_{sc} , a lower RAD of $16.3\% \pm 14.8\%$ was observed, followed by RAD values of $27.1\% \pm 20.6\%$ at 43 h and $27.2\% \pm 24.3\%$ at 69 h. Results for the spleen showed a mean RAD, with values ranging from $20.2\% \pm 14.9\%$ at 20 h, reaching the highest recorded value of $35.5\% \pm 48.8\%$ at 69 h t_{sc} .

The comparison between the iSTP and Hanscheid methods, including at 20, 43, and 69 h, showed no statistically significant differences across the assessed time points, except for the right kidney at 69 h t_{sc} ($P = 0.02$). For the left kidney at 20 h, the Hanscheid method achieved a mean RAD of $23.1\% \pm 13.1\%$, followed $13.8\% \pm 13.3\%$ and $8.1\% \pm 6.3\%$ at 43 and 69 h, respectively. A similar

pattern was observed for the right kidney, with $9.3\% \pm 12.4\%$ at 69 h t_{sc} . In liver and spleen measurements, the Hanscheid method obtained optimal RADs of $10.6\% \pm 9.0\%$ and $17.6\% \pm 11.8\%$, respectively, at 20 h t_{sc} .

Furthermore, we compared the iSTP early time points (2 and 20 h) for all organs with the optimal Hanscheid t_{sc} achieved at 69 h for the left and right kidneys and at 20 h for the liver and spleen. These findings are detailed in the Discussion section and are depicted in Supplemental Figure 1.

Robustness: Cycle Dependency

In the second scenario, we introduced the first cycle’s $^{68}\text{Ga-PSMA-11}$ PET data to predict T_{eff} for all subsequent therapy cycles, estimating the RAD in the absorbed dose. Two patient cycles were excluded because of missing information from the first cycle. The T_{eff} SVR model aggregated ME predictions of $27.8\% \pm 10.0\%$, $32.5\% \pm 10.1\%$, $24.1\% \pm 11.1\%$, and $20.5\% \pm 7.2\%$ for left and right kidneys, liver, and spleen, respectively. The nonpaired Mann–Whitney test, as shown in Figure 4, revealed no statistically significant differences ($P > 0.05$) in cycles 2, 3, and 4 or more across organs when comparing the predicted T_{eff} using pretherapy data obtained before each therapy cycle with the predictions from before the first-cycle scenario.

The estimated RADs in absorbed dose are illustrated in Figure 5, obtained from the second scenario. The differences by organ, categorized according to cycle, spanned from $14.6 \pm 8.7\%$ up to $30.8 \pm 19.8\%$ across all organs. Organ results were compared between both scenarios, showing no significant differences, consistently yielding P values greater than 0.05 (Supplemental Fig. 2).

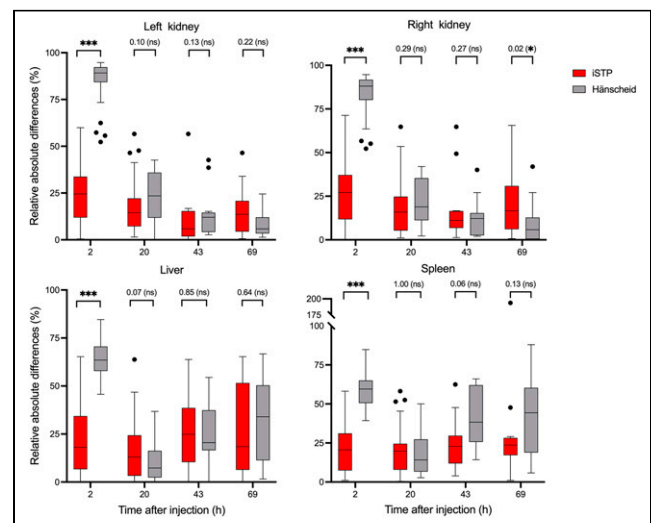


FIGURE 3. RADs in TIA by organ for both STP (iSTP and Hanscheid) methods compared with MTP method. Illustrated for left and right kidney, liver, and spleen at earlier postinjection time points (2 h*, 20 h, 43 h, and 69 h). *2 h t_{sc} is not applicable to Hanscheid method; included for comparison purposes. *** $P < 0.001$. ns = not significant.

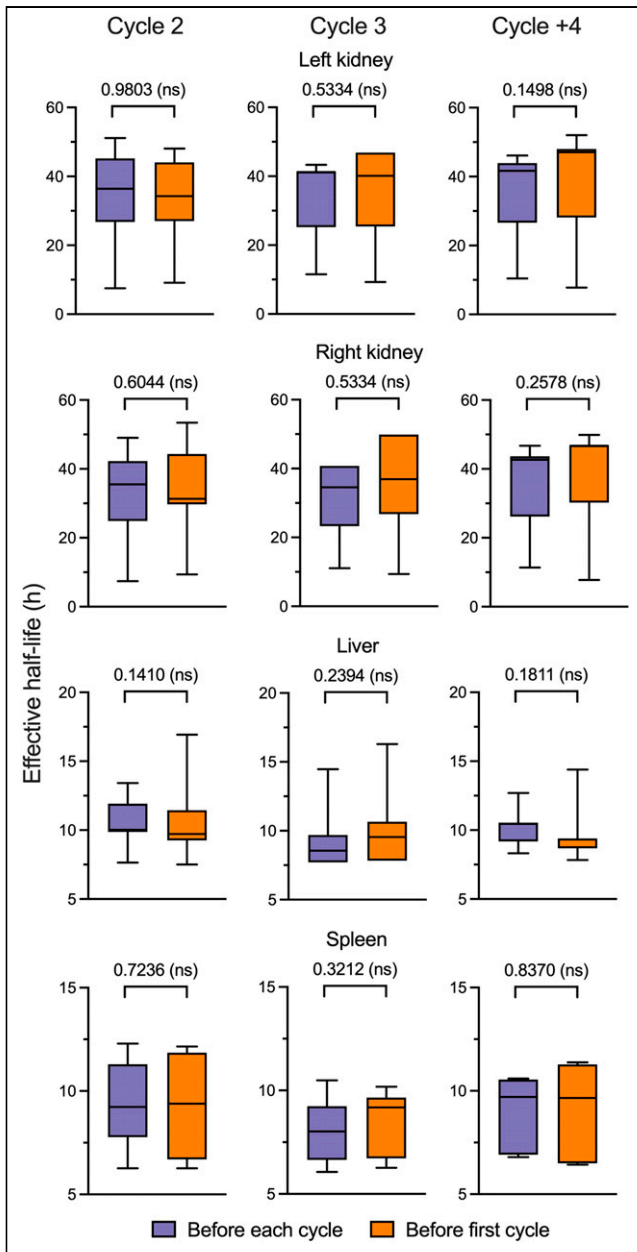


FIGURE 4. Statistical correlation between predicted T_{eff} when using pretherapy data before each cycle and before first cycle. Nonpaired Mann-Whitney test was performed for each therapy cycle, represented by columns, for left kidney, right kidney, liver, and spleen. ns = not significant.

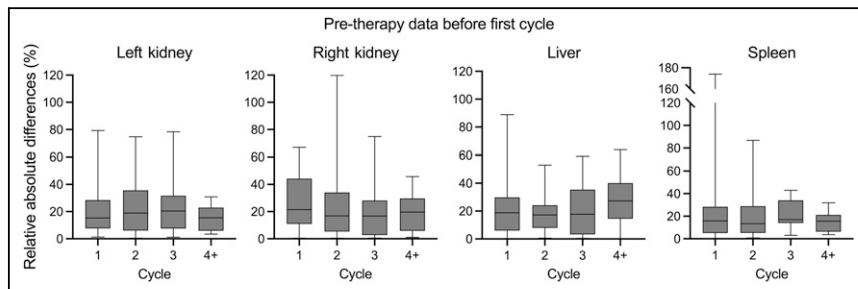


FIGURE 5. RADs in absorbed dose calculated and grouped by cycle using iSTP model from data preceding first therapy cycle.

DISCUSSION

A critical challenge in the practice of RPT is the dilemma of precision and clinic-friendly techniques. Finding a practical solution to implement dosimetry-guided personalization is difficult while allowing wide adoption in diverse routine scenarios. Particularly, outpatient treatment has become a mainstream practice in many countries, for which the conventional MTP method is unable to provide a flexible and convenient solution because of the strict requirement for a time point imaging acquisition window after therapy. However, although efficient, STP methods offer a limited measurement window because of their reliance on the time dependency of the scan time point.

The iSTP method aims to overcome these limitations arising from the STP, enabling early and flexible posttherapy scan times. It provides advantages for dosimetry assessment instantaneously after the patient starts the treatment, which is not practical because of the logistic challenges (5,8,13–15). iSTP can be achieved based on the knowledge that T_{eff} is an intrinsic characteristic of a patient's health status, integrating both the physical and the biologic half-life processes. The pretherapy patient imaging and clinical data provided valuable information about the patient's physiologic processes such as metabolism, clearance, and excretion (24), which can be used as features for predicting T_{eff} . Our investigation also confirms that these predictions, with an ME below 27%, have limited variations even during the therapy cycles, which introduced more physiologic alterations given sufficient pretherapy data, that is, data acquired ideally shortly before the treatment. Additionally, the inclusion of the SUV_{mean} from the urinary tract (kidneys and urinary bladder) and the clinical evaluation of the patient's organ conditions provided valuable insights for the model, as their classification significantly enhanced the prediction accuracy. The organ's TIA results obtained from iSTP compared with MTP in relative absolute differences, at different time points (2, 20, 43, and 69 h), for ^{177}Lu -PSMA I&T are presented in Figure 3.

Scan time limitation makes STP methods not feasible for dosimetry assessment at 2 h t_{sc} (5,12,25). Our iSTP method achieved a significant mean RAD of less than 27% for the left and right kidneys and liver, with differences below 20% for the same organs at 20 h t_{sc} . From a dosimetry perspective, we demonstrated the potential of this method for early and flexible scan acquisition for dose assessment compared with the standard MTP method.

By applying the Hånscheid method, based on the availability of this retrospective data, our findings align with the optimal performance reported in the literature for both kidneys (8,26). Although 2 h t_{sc} is not part of the Hånscheid method, we used it as a reference to demonstrate the instant capability of our method.

In Figure 3, we observe that the iSTP method outperformed the conventional method at 2 h, achieving statistical significance ($P < 0.001$) for all organs. Additionally, in Supplemental Figure 1, we show a comparison of the results between the early scan times at 2 h and 20 h for the iSTP method and the Hånscheid method at optimal time points (69 h for the left and right kidneys and 20 h for the liver and spleen). Our analysis revealed that iSTP early time points showed significant differences compared

with another method for the left and right kidneys ($P < 0.05$). A similar pattern was seen for the liver at 2 h, though at 20 h, the difference was not significant ($P = 0.07$). No significant difference was observed for the spleen at either time point. Overall, our method performed comparably or better than the Hanscheid method, demonstrating an improved accuracy in certain scenarios considering time point dependency.

Contrary to conventional STP methods, which suffer from large dosimetric variances in the first hours, our method demonstrated an early scan posttherapy point of choice for the left and right kidneys, liver, and spleen. However, significant outliers were identified. Notably, at 2 h t_{sc} for both kidneys, outliers were identified in a few patients with differences exceeding 60%. We noted that 1 patient had liver metastasis, normal function in the right kidney, and bone metastasis after treatment. Although these unexpected values may arise from factors such as patient clinical status and estimation of T_{eff} , suggesting a low level and rapid clearance of activity uptake at earlier time points, they may be associated with fitting and prediction errors. The study by Xue et al. (20) illustrated that the liver exhibited the highest level of radiopharmaceutical accumulation within the body, showcasing the most rapid decrease in radioactivity. The same behavior was observed for the spleen. Such pharmacokinetic inaccuracies potentially compromise the reliability of radiation dose assessments for the liver and spleen at 69 h t_{sc} (13,27). Early time points are less influenced by metabolic and clearance processes that can introduce variability. The activity of the radiotracer is higher at early time points, resulting in a better signal-to-noise ratio for imaging and measurements. As the radiotracer decays over time, the signal diminishes, and the influence of background noise and statistical fluctuations increases, leading to significant variability and impracticality of dosimetry at late time points (Supplemental Fig. 3). Highlighting the significance of activity uptake is crucial for understanding the impact it has on the dosimetry process.

The salivary gland would ideally be a key focus as an organ at risk in PSMA RPT. In this retrospective study, it was not included in the field of view during the SPECT acquisition. Nonetheless, the proof of concept in current normal organs paves the way for future studies on other organs using this clinically friendly dosimetry approach.

In the second scenario, the SVR model predicted the T_{eff} with an ME ranging from 20% to 32%, averaging a 4% difference from the first scenario for the left and right kidneys and being similar to that for the liver and spleen. However, with the dosimetry analysis grouped by cycle in both scenarios, no statistically significant differences were observed in all grouped cycles. Nonetheless, the mean RAD in absorbed dose indicated a minimum value for the left kidney in cycle 4 and further and a maximum for the liver for the same cycle. This scenario would enable a careful evaluation of using the predicted T_{eff} obtained before the first cycle for dosimetry in subsequent cycles. However, to assess the robustness of the model, further validation of our data is required.

The STP method has its limitations in accurately assessing dosimetry at early and later postinjection t_{sc} , as mentioned previously. On the other hand, the iSTP method targets its application for early time points optimally within the first or even second day after injection, which is generally more practical for dosimetry implementation in outpatient or short-duration inpatient treatment. This is still a challenge for predicting T_{eff} for the late cycles. A common assumption that biokinetics and dosimetry remain constant across cycles is a debated topic. Supporting this, Malcom

et al. (28) found a 30% increase in kidney T_{eff} between cycles, significantly affecting dose predictions.

This study faced several limitations. First, we acknowledge that the small sample size significantly affected the results, leading to inaccurate predictions, fitting issues, and higher variations. We observed more outliers than the conventional STP method. The machine learning model can be improved by incorporating more patient data for training. Future work should aim to increase the sample size to achieve a more robust statistical power. Second, our patient data are limited to 1 bed position of the abdominal region and do not include all critical organs and lesions. Future work that includes other organs and lesions is desired. Despite these limitations, our preliminary findings highlight the potential of the proposed iSTP method to simplify and promote routine clinical dosimetry implementation.

CONCLUSION

The proposed iSTP method simplifies dosimetry and demonstrates flexibility in selecting early posttreatment imaging time points. Preliminary results indicate that, despite fluctuations in relative absolute differences, our iSTP method effectively predicts the T_{eff} using pretherapy data and facilitates STP measurement shortly after RPT. This method could expedite the broader application of dosimetry in both outpatient and short-duration inpatient treatments.

DISCLOSURE

Financial support was funded by Swiss National Science Foundation (grant no. 188914). Kuangyu Shi and Axel Rominger receive research grants from Novartis and Siemens Healthineers. No other potential conflict of interest relevant to this article was reported.

KEY POINTS

QUESTION: Can early postscan imaging be used for STP dosimetry?

PERTINENT FINDINGS: Our study demonstrated that incorporating pretherapy data from each cycle and before the first therapy cycle enabled the prediction of organ-specific T_{eff} for PSMA RPT. The iSTP method was evaluated against MTP and STP approaches, highlighting its achievement at early and flexible 2 h and 20 h t_{sc} for dosimetry after therapy. However, careful evaluation is advised when using PET/CT data from before the first therapy cycle to predict outcomes in subsequent cycles.

IMPLICATIONS FOR PATIENT CARE: The iSTP method paves the way for improved patient care by ensuring dosimetry assessment is completed before the patient leaves the center after treatment administration.

REFERENCES

1. Kratochwil C, Fendler WP, Eiber M, et al. EANM procedure guidelines for radionuclide therapy with ^{177}Lu -labelled PSMA-ligands (^{177}Lu -PSMA-RLT). *Eur J Nucl Med Mol Imaging*. 2019;46:2536–2544.
2. Sjogreen Gleisner K, Chouin N, Gabina PM, et al. EANM dosimetry committee recommendations for dosimetry of ^{177}Lu -labelled somatostatin-receptor- and PSMA-targeting ligands. *Eur J Nucl Med Mol Imaging*. 2022;49:1778–1809.

3. Gear J, Stokke C, Terwinghe C, et al. Correction to: EANM enabling guide: how to improve the accessibility of clinical dosimetry. *Eur J Nucl Med Mol Imaging*. 2023;50:3157–3158.
4. Council Directive 2013/59/EURATOM of 5 December 2013 laying down basic safety standards for protection against the dangers arising from exposure to ionising radiation, and repealing Directives 89/618/Euratom, 90/641/Euratom, 96/29/Euratom, 97/43/Euratom and 2003/122/Euratom. EUR-Lex website. <https://eur-lex.europa.eu/legal-content/de/TXT/?uri=CELEX%3A32013L0059>. Updated January 17, 2014. Accessed March 6, 2025.
5. Madsen MT, Menda Y, O'Dorisio TM, O'Dorisio MS. Technical note: Single time point dose estimate for exponential clearance. *Med Phys*. 2018;45:2318–2324.
6. Devasia TP, Dewaraja YK, Frey KA, Wong KK, Schipper MJ. A novel time-activity information-sharing approach using nonlinear mixed models for patient-specific dosimetry with reduced imaging time points: application in SPECT/CT after ^{177}Lu -DOTATATE. *J Nucl Med*. 2021;62:1118–1125.
7. Hardiansyah D, Riana A, Beer AJ, Glatting G. Single-time-point dosimetry using model selection and nonlinear mixed-effects modelling: a proof of concept. *EJNMMI Phys*. 2023;10:12.
8. Brosch-Lenz J, Delker A, Völter F, et al. Towards single time point image-based dosimetry of ^{177}Lu -PSMA-617 therapy. *J Nucl Med*. 2023;64:767–774.
9. Peters SMB, Mink MCT, Prive BM, et al. Optimization of the radiation dosimetry protocol in lutetium-177-PSMA therapy: toward clinical implementation. *EJNMMI Res*. 2023;13:6.
10. Stokke C, Gabina PM, Solny P, et al. Dosimetry-based treatment planning for molecular radiotherapy: a summary of the 2017 report from the Internal Dosimetry Task Force. *EJNMMI Phys*. 2017;4:27.
11. Gay HA, Michalski JM. Radiation therapy for prostate cancer. *Mo Med*. 2018;115:146–150.
12. Hanscheid H, Lapa C, Buck AK, Lassmann M, Werner RA. Dose mapping after endoradiotherapy with ^{177}Lu -DOTATATE/DOTATOC by a single measurement after 4 days. *J Nucl Med*. 2018;59:75–81.
13. Jackson PA, Hofman MS, Hicks RJ, Scalzo M, Violet J. Radiation dosimetry in ^{177}Lu -PSMA-617 therapy using a single posttreatment SPECT/CT scan: a novel methodology to generate time- and tissue-specific dose factors. *J Nucl Med*. 2020;61:1030–1036.
14. Hou X, Brosch J, Uribe C, et al. Feasibility of single-time-point dosimetry for radiopharmaceutical therapies. *J Nucl Med*. 2021;62:1006–1011.
15. Peterson AB, Miranda DM, Dewaraja YK. Accuracy and uncertainty analysis of reduced time point imaging effect on time-integrated activity for ^{177}Lu -DOTATATE PRRT in patients and clinically realistic simulations. *EJNMMI Res*. 2023;13:57.
16. Kratochwil C, Fendler WP, Eiber M, et al. Joint EANM/SNMMI procedure guideline for the use of ^{177}Lu -labeled PSMA-targeted radioligand-therapy (^{177}Lu -PSMA-RLT). *Eur J Nucl Med Mol Imaging*. 2023;50:2830–2845.
17. Huang HL, Tong AKT, Thang SP, et al. Current status and growth of nuclear theranostics in Singapore. *Nucl Med Mol Imaging*. 2019;53:96–101.
18. Andrade C. The practical importance of half-life in psychopharmacology. *J Clin Psychiatry*. 2022;83:22f14584.
19. Okamoto S, Thieme A, Allmann J, et al. Radiation dosimetry for ^{177}Lu -PSMA I&T in metastatic castration-resistant prostate cancer: absorbed dose in normal organs and tumor lesions. *J Nucl Med*. 2017;58:445–450.
20. Xue S, Gafita A, Dong C, et al. Application of machine learning to pretherapeutically estimate dosimetry in men with advanced prostate cancer treated with ^{177}Lu -PSMA I&T therapy. *Eur J Nucl Med Mol Imaging*. 2022;49:4064–4072.
21. Bolch WE, Eckerman KF, Sgouros G, Thomas SR. MIRD pamphlet No. 21: a generalized schema for radiopharmaceutical dosimetry—standardization of nomenclature. *J Nucl Med*. 2009;50:477–484.
22. Montesinos Lopez OA, Montesinos Lopez A, Crossa J. *Multivariate Statistical Machine Learning Methods for Genomic Prediction*. Springer; 2022.
23. Guido R, Ferrisi S, Lofaro D, Conforti D. An overview on the advancements of support vector machine models in healthcare applications: a review. *Information*. 2024;15:235.
24. Yeong CH, Cheng MH, Ng KH. Therapeutic radionuclides in nuclear medicine: current and future prospects. *J Zhejiang Univ Sci B*. 2014;15:845–863.
25. Rinscheid A, Kletting P, Eiber M, Beer AJ, Glatting G. Influence of sampling schedules on ^{177}Lu Lu-PSMA dosimetry. *EJNMMI Phys*. 2020;7:41.
26. Wang C, Peterson AB, Wong KK, Roseland ME, Schipper MJ, Dewaraja YK. single-time-point imaging for dosimetry after [^{177}Lu]Lu-DOTATATE: accuracy of existing methods and novel data-driven models for reducing sensitivity to time-point selection. *J Nucl Med*. 2023;64:1463–1470.
27. Hollriegl V, Petoussi-Henss N, Hurkamp K, Ocampo Ramos JC, Li WB. Radiopharmacokinetic modelling and radiation dose assessment of ^{223}Ra used for treatment of metastatic castration-resistant prostate cancer. *EJNMMI Phys*. 2021;8:44.
28. Malcolm JC, Falzone N, Gains JE, et al. Impact of cyclic changes in pharmacokinetics and absorbed dose in pediatric neuroblastoma patients receiving [^{177}Lu]Lu-DOTATATE. *EJNMMI Phys*. 2022;9:24.